DISPOSAL OF LIBRATION POINT ORBITS ON A HELIOCENTRIC GRAVEYARD ORBIT: THE GAIA MISSION

Camilla Colombo[(1)], **Francesca Letizia**[(2)], **Stefania Soldini**[(3)] **and Florian Renk**[(4)]
[(1)(2)(3)] *Aeronautics, Astronautics and Computational Engineering Unit, University of Southampton, SO171BJ, UK, c.colombo@soton.ac.uk.*
[(4)] *ESA/ European Space Operations Centre, 64293 Darmstadt, Germany.*

Abstract: *This paper presents the options for Gaia disposal through transfer into a heliocentric graveyard orbit. The disposal manoeuvre sequence is designed in a high-fidelity dynamical model using an energetic approach written in the osculating restricted three-body problem. A first manoeuvre is given to leave the Libration Point Orbit, while a second manoeuvre is used to decrease the three-body problem energy of the spacecraft. The disposal design is optimised to maximise the distance from Earth for a period of 100 years and to minimise the possibility of gravitational interaction with the Earth, due to perturbation induced by other planets. Particular emphasis is given to the effect of the eccentricity of the Earth's orbit around the Sun. The elliptical restricted three body problem formulation and the results in the full dynamics are used to show the dependence of the manoeuvre to the angular position of the Earth-Moon barycentre with respect to the Sun at the time of injection into the disposal trajectory. These findings are exploited to design a novel disposal strategy that is sustainable and minimises the chance of return to Earth on the long term.*

Keywords: *End-of-life disposal, graveyard orbit, trajectory optimisation, restricted three body problem, elliptical restricted three body problem.*

1. Introduction

Libration Point Orbits (LPOs) in the Sun-Earth system are used for astronomy missions, such as Herschel, Planck, SOHO, and Gaia, and future missions, such as Euclid, ATHENA, PLATO will also use this type of orbits. Indeed, LPOs have a stable geometry with respect to the Sun and the Earth, thus offering a vantage point for the observation of the Sun and the Universe, together with optimal operating condition in terms of radiation environment, telecoms and thermal design. In addition, the amount of propellant to target orbits around the Libration Points L_1 and L_2 is low compared to alternative orbits.

Recent studies funded by the European Space Agency (ESA) [1-3] highlighted the importance of considering the end-of-life disposal since the early stages of the mission design to define a sustainable strategy for the disposal with the objective of avoiding interference with the Geostationary and Low Earth Orbit protected regions and minimising the event of an uncontrolled re-entry within the Earth's atmosphere several years after the operational mission end. Three possible options have been considered for end-of-life disposal of LPOs: disposal through a semi-controlled Earth re-entry [4], disposal through impact onto the lunar surface or transfer into a graveyard heliocentric orbit. The latter strategy was already implemented for ISEE-3/ICE, Planck and Herschel.

This paper will analyse the options for Gaia disposal through transfer into a heliocentric graveyard orbit. The disposal manoeuvre sequence is designed in a high-fidelity dynamical model using an energetic approach written in the osculating restricted three-body problem. A

first manoeuvre is given to leave the LPO, while a second manoeuvre is used to decrease the three-body problem energy of the spacecraft. The disposal design is optimised to maximise the distance from Earth for a period of 100 years and to minimise the possibility of gravitational interaction with the Earth, due to perturbation induced by other planets. Moreover, the Elliptical Restricted Three Body Problem formulation is used to show the dependence on the sensitivity of the manoeuvre to the angular position of the Earth-Moon barycentre with respect to the Sun. The aim of this work is to understand how the dynamics influences the efficiency of the disposal manoeuvre. The findings are exploited to design a novel disposal strategy, based that is sustainable and minimises the chance of return to Earth on the long term.

The paper is organised as follows, Section 2 summarises the method for the heliocentric disposal manoeuvre design by closing the Hill's curves in the Circular Restricted Three Body Problem (CRTBP), proposed by Olikara et al. [5] and applied to three ESA missions, namely Herschel, SOHO and Gaia in [2]. The trajectory design method considering the high-fidelity dynamical model, is presented in Section 3. The optimisation of the manoeuvre sequences is explained in Section 3.2, where a novel strategy is devised, based on the analysis of close approaches, which allows having a robust and sustainable disposal. Section 4 gives the Gaia mission parameters needed for the design of its end-of life. The results are presented in Section 5. The effects of the Earth's eccentricity are also analysed through an analytical approach based on the Elliptical Restricted Three Body Problem model in Section 6.

2. Heliocentric disposal manoeuvre design in the CR3BP

When considering the disposal of spacecraft in LPOs, the main requirement is that the spacecraft does not return to the Earth for at least 100 years after the disposal epoch [3]. As demonstrated by analyses performed in the Circular Restricted Three Body Problem (CRTBP), a small manoeuvre is enough to inject the spacecraft into the unstable manifold leaving the Earth's vicinity though L_2. However, a second manoeuvre is needed to ensure that the trajectory will not return towards the Earth. To this aim, an energetic approach in the CRTBP was originally proposed by Olikara et al. [6]. This approached was applied to three selected ESA missions in [1-3]. In these studies, the circular restricted three body problem was adopted, considering the Sun and the Earth + Moon as primary masses.

For any point expressed in the synodic system of the Circular Restricted Three Body Problem (CR3BP) the Jacoby constant can be computed as [7]:

$$J\left(\mathbf{s}_{\text{syn}}\right) = -\left(\dot{x}^2 + \dot{y}^2 + \dot{z}^2\right) + x^2 + y^2 + 2\left(\left(1-\beta\right)\frac{1-\mu}{r_S} + \frac{\mu}{r_E}\right) \tag{1}$$

where $r_S = \sqrt{\left(x+\mu\right)^2 + y^2 + z^2}$ and $r_E = \sqrt{\left(x+\mu-1\right)^2 + y^2 + z^2}$ describe the spacecraft position from the Sun and the Earth, respectively and $\mathbf{s}_{\text{syn}} = \begin{bmatrix} x & y & z & \dot{x} & \dot{y} & \dot{x} \end{bmatrix}$ is the state vector in the synodic system. The lightness parameter β is included to consider the effect of solar radiation pressure as function of the area-to-mass ratio and the reflective coefficient of the spacecraft.

One first infinitesimal manoeuvre was considered in [1, 2, 6] to inject the spacecraft into the unstable manifold leaving the LPO through L_2, and the second manoeuvre was determined imposing that the Jacoby constant, once the manoeuvre is given, has to be increased, at least, to the value of J_{L_2}, to ensure that the Hill's curve are closed in correspondence of the L_2 point, thus

preventing the spacecraft to return back to the Earth's region. Eq. (1) can be evaluated at the Libration point L_2 to define J_{L_2}.

Considering a trajectory that departs from the LPO through L_2, the Hill's curves are initially opened at L_2, i.e., $J < J_{L_2}$. The velocity after the first manoeuvre for leaving the LPO can be computed inverting Eq. (1) as $\left(v^2\right)^- = \left(\dot{x}^2 + \dot{y}^2 + \dot{z}^2\right) = x^2 + y^2 + 2\left(\left(1-\beta\right)\frac{1-\mu}{r_S} + \frac{\mu}{r_E}\right) - J$.

Now, at a position beyond L_2, a second manoeuvre is given to close the zero-velocity curves. In other words, the required velocity after the manoeuvre can be determined by imposing that $J\left(\mathbf{s}_{\text{syn}}\right)$ equals J_{L_2}:

$$\left(v^2\right)^+ = x^2 + y^2 + 2\left(\left(1-\beta\right)\frac{1-\mu}{r_S} + \frac{\mu}{r_E}\right) - J_{L_2} \tag{2}$$

Since the curves are opened at time $t^-_{\Delta v_2}$ and closed at time $t^+_{\Delta v_2}$, this means that $\left(v^2\right)^- > \left(v^2\right)^+$: the second manoeuvre needs to increase the Jacobi constant (i.e., decrease the energy since $J = -2E$), therefore the absolute value of the minimum required Δv to close the Hill's curves at L_2 is

$$\Delta v_{\text{closure @ } J_2} = v^- - v^+ \tag{3}$$

and it has to be given in the opposite direction to the initial velocity $\mathbf{v}^-$.

Note that, given a position in the synodic frame beyond L_2, the best condition of curve closure would be such that, not only the curves are closed at L_2 (i.e., $J = J_{L_2}$), but a more conservative closure is achieved such that $J > J_{L_2}$. The most conservative condition is when the velocity after the Δv manoeuvre is zero: $v^+ = 0$, which means that the spacecraft is at the boundary of the forbidden region, so it is well prevented from reaching L_2. This allows defining the most conservative condition for closure at the boundary of the forbidden region:

$$\Delta v_{\text{closure @ } FR} = v^- = \sqrt{\dot{x}^2 + \dot{y}^2 + \dot{z}^2} \tag{4}$$

Finally, note that, as shown by Olikara et al. [6], it is not possible to close the Hill's curve at any position; in particular in some cases the spacecraft can be, after the Δv manoeuvre, inside the forbidden regions. Therefore, a filter was added in [3] to identify the boundaries of the forbidden regions as

$$J < J^* \tag{5}$$

where, J is the Jacoby constant, while J^* is the critical Jacobi constant, i.e., when the velocity in the Synodic system is zero:

$$J^* = (x^2 + y^2) + 2\left(\left(1-\beta\right)\frac{1-\mu}{r_S} + \frac{\mu}{r_E}\right)$$

The reader is invited to refer to Olikara et al. [6] for a more detailed explanation of the disposal manoeuvre in the CRTBP and to [3] for the result of this analysis on three selected ESA missions: Herschel, SOHO and Gaia.

3. Heliocentric disposal manoeuvre design in the full-ephemerides model

The aim of this work is to:

- design the heliocentric disposal in a full dynamical model;
- design a robust disposal that prevents the return of the spacecraft to Earth for the following 100 years at least
- analyse the effect of the Earth's eccentricity and the other perturbations on the disposal strategy
- analyse the behaviour of the close approaches between spacecraft and Earth once the disposal manoeuvre is given

3.1. High-fidelity model of the dynamics

The heliocentric disposal for Gaia was designed in the full dynamical model, considering the effects of Solar Radiation Pressure (SRP), the Earth's oblateness and the planets gravitational attraction. For SRP, a cannonball model was used, with the Sun position computed from the ephemerides. No eclipses are considered at this stage. The planets considered for the disposal design are: Earth, Mercury, Venus, Mars, Jupiter, Moon, and the Sun. NASA Horizon ephemerides (JPL_D405) are used with interpolation with Chebyshev polynomials. The dynamics is centred at the Earth in an equatorial inertial reference system.

The trajectory is integrated using a variable order Adams-Bashforth-Moulton PECE (Predict-Evaluate-Correct-Evaluate) solver, implemented in the Matlab function `ode113`.

For the evaluation of the Jacobi constant, for each time step the trajectory is transformed into the osculating Restricted Three Body Problem (R3BP), centred at the barycentre of the Sun – Earth + Moon system, with the *x*-axis in the instantaneous direction from the Sun to the Earth + Moon. This means that the *x*-y plane is not uniformly rotating around the *z*-axis.

The position of the spacecraft in the non-dimensional synodic reference $\mathbf{r}_{\text{syn}}$ frame is expressed as:

$$\mathbf{r}_{syn} = M^T \frac{\mathbf{r}_{sid}}{k}$$

where, M is the direction cosine matrix, $\mathbf{r}_{\text{sid}}$ is give from Gaia's ephemeris and k is the Earth-Sun distance, $\|\mathbf{r}_{E-S}\|$. The velocity is given by deriving $\mathbf{r}_{\text{syn}}$ as a function of time and by adimensionalising the velocity for the angular velocity:

$$v_{syn} = \left[M^T \frac{v_{sid}}{k} + \dot{M}^T \frac{r_{sid}}{k} - M^T r_{sid} \frac{r_{E-S} \times v_{E-S}}{\|r_{E-S}\|^3} \right] \frac{\|r_{E-S}\|}{\|v_{E-S}\|}$$

where $r_{E-S} = \|r_{E-S}\|$ and $\|\mathbf{v}_{E-S}\| = \sqrt{\mu_{E-S}/r_{E-S}}$ introducing the hypothesis of mean motion of the Earth around the Sun.

3.2. Disposal manoeuvre design

Given a starting time t_0 and state $\mathbf{s}_0$ on the nominal LPO, a first manoeuvre $\Delta\mathbf{v}_1$ is performed to leave the LPO along an unstable outbound trajectory. The state on the LPO after $\Delta\mathbf{v}_1$ is propagated for the time interval Δt_1 and the first trajectory leg of the trajectory Leg 1 is computed in the sidereal reference frame. To ensure that the trajectory is outbound, all the trajectories which reach, at any point, a distance from Earth less than $1.2 \cdot 10^6$ km are discarded

(note that the minimum distance of the nominal LPO from Earth is $1.3667 \cdot 10^6$ km). Moreover, another check is performed on the final state of Leg 1 to ensure its *x*-component in the synodic frame is higher than x_{L_2}.

At this point, a second manoeuvre $\Delta\mathbf{v}_2$ is given with the aim of increasing the value of the Jacobi constant. The initial state on Leg 2 is propagated up to $t_0 + \Delta t_1 + \Delta t_{EOL}$ and the value of the Jacobi constant along the second leg $J_{\text{leg 2}}\left(\mathbf{s}_{\text{leg 2, syn}}\right)$ is calculated through Eq. (1) to compute the objective function. The trajectory optimisation is performed using the following optimisation parameters:

$$\mathbf{y} = \left[\eta_{\Delta v_1} \quad \alpha_1 \quad \beta_1 \quad \Delta t_1\right]$$

where $\eta_{\Delta v_1}$ is the fraction of the maximum available Δv used in the first manoeuvre, α_1 is the right ascension (in-plane angle) of the Δv in the synodic frame for the first manoeuvre Δv_1, β_1 is the elevation angle of the Δv in the synodic frame for the first manoeuvre Δv_1, Δt_1 is the time interval between the two manoeuvres, limited to a maximum of six months.

The second manoeuvre $\Delta\mathbf{v}_2$ is performed using all the remaining available $\Delta v_{2,\text{avl}}$ rescaled considering the efficiency of the manoeuvre (that depends on its direction). At this point two considerations can be made: if $\Delta v_{2,\text{avl}} < \Delta v_{\text{closure @ J}_2}$ (where $\Delta v_{\text{closure @ J}_2}$ is defined in Eq. (3)), the closure at L_2 is not feasible. Moreover, if seen in the synodic frame, the most conservative case would be when $\Delta v_{\text{avl}} = \Delta v_{\text{closure @ FR}}$ (in Eq. (4)), which means that, after the second manoeuvre, the spacecraft is at the boundary of the forbidden region. Therefore, a check is present to guarantee that the Δv_2 does not exceed $\Delta v_{\text{closure @ FR}}$: $\Delta v_2 = \min\left[\Delta v_{2,\text{avl}},\ \Delta v_{\text{closure @ FR}}\right]$.

Moreover, for the second manoeuvre α_2 and β_2 are fixed with respect to the velocity measured in the synodic system and respectively equal to π and 0 (with respect to the velocity in the synodic system). In this case, in fact, we want to increase the value of the Jacobi constant, which correspond to decrease the velocity at the beginning of Leg 2. As a consequence we give $\Delta\mathbf{v}_2$ against the velocity itself.

Of course, fixing the angles of the second manoeuvre is an approximation because:

- we are in a R3BP osculating synodic frame, therefore it is expected that, due to the presence of other perturbations, the direction that decreases the total energy can be off the anti-tangential direction;
- the efficiency of the manoeuvre depends on the manoeuvre direction, therefore a manoeuvre off the anti-tangential direction may be more efficient in terms of propellant consumption.

However, this choice allows decreasing the computational time as the parameter space is reduced. Finally, note that, both Δv_1 and Δv_2 are rescaled according to the efficiency of the manoeuvre, which depends on the direction of the manoeuvre with respect to the Δv-to-Sun angle, as will be shown in Section 4. The upper and lower boundaries for the design parameter $\mathbf{y}$ are taken equal to:

$$\mathbf{y}_{\text{LB}} = \left[0 \quad -\pi \quad -\pi/2 \quad 0.01 \cdot 365.25\right]$$

$$\mathbf{y}_{\text{UB}} = \left[1 \quad \pi \quad \pi/2 \quad 0.5 \cdot 365.25\right]$$

The objective function is set equal to

$$\phi = k \log \frac{J_{L_2}}{J_{\text{leg 2, min}}} + P \tag{6}$$

where $P = 10^{20}$ is a penalty factor that is assigned to solutions that

- arrive too close to the Earth (their distance from the Earth is lower than the one between the Earth and L_2)
- have allocated for the second manoeuvre a Δv lower than the one required to close the zero-velocity curve as explained above.
- have entered the forbidden regions as in Eq. (5).

Given the definition of ϕ, negative values indicate solutions where the minimum J in the monitored points is higher than J at L_2. The set of points to check can be defined in two different ways:

- Case 1: all points along the trajectory:

$$J_{\text{leg 2, min}} = \min\left(J_{\text{leg 2}}\left(\mathbf{s}_{\text{leg 2, syn}} \right) \right)$$

- Case 2: only the points of close approach with the Earth are checked, where *close approach* is defined as a point where:

$$CA: \; x_{\text{leg 2, syn}} > 0 \quad \& \quad \left| y_{\text{leg 2, syn}} \right| < 10^{-2}$$

$$J_{\text{leg 2, min}} = \min\left(J_{\text{leg 2}}\left(\mathbf{s}_{\text{leg 2, syn}} @ \text{CA} \right) \right) \tag{7}$$

The optimisation performed with in the Case 1 is more general, but it was observed that the optimiser was never able to find a solution always above J_{L_2} for the entire time window along Leg 2. It was therefore preferred to adopt the Case 2 approach in order to improve the solutions in the points where is actually relevant to control the energy value of the trajectory.

The time window chosen for the propagation of Leg 2 was set equal to Δt_{EOL} 30 years to reduce the computational time; the optimised solutions (over 30 years) are then checked again also with a longer propagation to cover 100 years of the trajectory evolution.

Note that another option for the optimisation of the disposal trajectory would have been to simply maximise the minimum distance achieved from Earth. This would have simplified the manoeuvre computation as the transformation to the osculating synodic system would not be required for each time step. However, it was decided not to follow this route as measuring the disposal efficiency in terms of J allows measuring the third body effect of the Earth (in terms of $J_{\text{leg 2, min}} - J_{L_2}$). The minimum distance achieved from Earth was anyway computed in post-processing and used as ranking criterion for the solutions.

The trajectory optimisation was performed using genetic algorithms, considering a population of 50 individuals and a maximum of 100 generations. The tournament selection is applied to identify the best individuals and the mutation is used 10% of the times to maintain genetic diversity. The simulation were run in Matlab, with core parallelisation on 12 cores. Each simulation required approximately 11 hours computational time.

The starting time of the disposal phase is not included in the optimisation with the genetic algorithm, but it treated performing a grid search along all the possible values considering the

given constraints. For each selected stating point, the optimisation with the genetic algorithm is launched. Many cases were optimised, corresponding to different starting points on the LPO distributed across all the possible values both in time and in true anomaly at the starting point on the LPO.

4. Gaia orbit and spacecraft parameters

The ephemerides of Gaia spacecraft were provided by ESA, until 17/06/2014, while the predicted one were downloaded from NASA Horizon system[1].

4.1. Gaia eclipse avoidance manoeuvre

The nominal trajectory will have an eclipse at 7167.459 MJD2000 (16/8/2019) and thus an eclipse avoidance manoeuvre is implemented by changing the phase angle as derived by Canalias [5]. Both in-plane and out-of-plane manoeuvres were implemented. The amplitudes for the manoeuvres were computed as the average of the actual amplitudes from the ephemerides in the range 2013-Dec-19 to 2019-Jun-20 and the estimated one obtained with the full body propagation [4]. Thereafter, the amplitudes are considered as constant.
Some assumptions are made:

- The amplitudes used for the manoeuvres are the average of the actual amplitudes from the ephemerides in the range 2013-Dec-19 to 2019-Jun-20.
- No manoeuvre constraints were considered for the eclipse avoidance manoeuvre, rather some manoeuvre efficiency are taken into account.
- After the eclipse avoidance manoeuvre, Gaia orbit is propagated in the linearised model, using amplitudes and phases right after the manoeuvre. No orbit control is applied thereafter. The reason for this assumption is that this will represent the target orbit for the station keeping control.

Figure 1 shows the out-of-plane and the in-plane phase angle manoeuvres. The grey crosses represent the evolution on the effective phase plane as from NASA Horizon[2], the blue crosses represent the evolution with the linearised system; the exclusion zone are marked in black; the red dot identifies the point where the manoeuvre starts and the green one where it ends.
The theoretical Δv for the manoeuvres is computed as in [8] and the values are reported in Table 1 (Δv_{th}): the out-of-plan manoeuvre is the cheapest and so it is the one implemented. The actual Δv (Δv_{ac}) is computed considering the thrust efficiency (η), which depends on the Δv to Sun angle[3] as shown in Figure 2. The out-of-plane manoeuvre was selected and was then refined in the full-body problem. The propagation in the full-body problem is carried out for an interval of time and then the analytical (linearised) method is applied (this is due to the fact that the full-body orbit should be controlled).

---

[1] Jet Propulsion Laboratory, "Horizons Web-Interface". [Online]. Available: http://ssd.jpl.nasa.gov/horizons.cgi [Last accessed: 03/07/2014]

[2] Jet Propulsion Laboratory, "Horizons Web-Interface". [Online]. Available: http://ssd.jpl.nasa.gov/horizons.cgi [Last accessed: 03/07/2014]

[3] Renk F., personal communication – email, 10 June 2014.

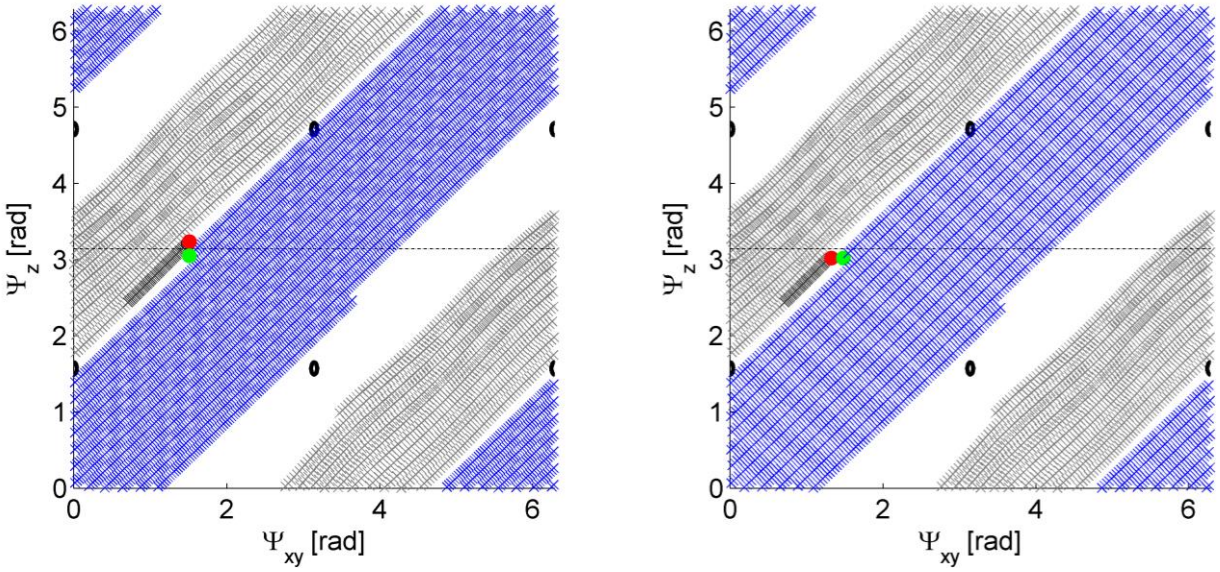

a) *b)*

Figure 1. Eclipse avoidance manoeuvre: a) out-of-plane manoeuvre, b) In plane manoeuvre

Table 1. Gaia eclipse avoidance manoeuvres.

Manoeuvre	Δv_{th} [m/s]	η [%]	Δv_{ac} [m/s]	Time [MJD2000]	Date
Out-of-plane manoeuvre (theoretical)	12.708	78.35	16.219	7125.591	05/07/2019
Out-of-plane manoeuvre (refined full-body problem)	10.039	78.35	12.813	7125.183	05/07/2019
In-plane manoeuvre (theoretical)	21.187	62.86	33.706	7119.302	29/06/2019

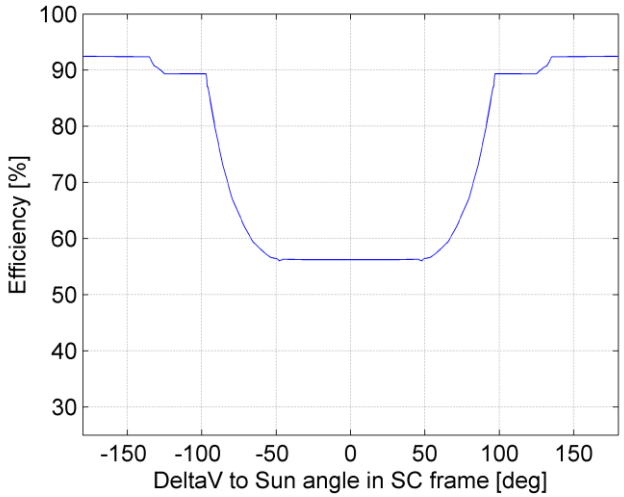

Figure 2. Thrust efficiency (η) as function of the Δv to Sun angle.

4.2. Gaia disposal requirements

The requirements for the disposal are:

- The time window for starting the disposal manoeuvre for GAIA is 1 July 2019 to 31 December 2020.
- The manoeuvre efficiency is represented in Figure 2.
- The propellant constraints are described below.

The total available Δv is measured according to the annual consumption of 1.32 m/s and the required Δv for the eclipse avoidance manoeuvre of 12.813 m/s for eclipse avoidance (on 05/07/2019). Since the propellant estimation for the end-of-life of Gaia were updated by the operations team during the study, two values were considered for the trajectory design:

A. Available Δv_{EOL} of 343.52014 m/s (corresponding to a propellant mass of 184.8056 kg) on 06/07/2019 (i.e., after the eclipse avoidance manoeuvre) as in Table 2.
B. Available Δv_{EOL} of 218.74 m/s (corresponding to a propellant mass of 115 kg) on 06/07/2019 (i.e., after the eclipse avoidance manoeuvre) as in Table 3.

Finally, note that, in both cases, 0.8 of the maximum available velocity is used as upper limit of the available Δv, as a 20% is left as margin for correction manoeuvres.

Table 2. Gaia Δv of 12.813 m/s for eclipse avoidance on 05/07/2019.

EOL epoch	Available Δv [m/s]	Fuel mass [kg]	Total mass [kg]	A/m [m^2/kg]	$c_R^* \cdot A/m$ [m^2/kg]
04/07/2019	356.2086	192.08	1584.08	0.05158	0.062498
06/07/2019	343.52014	184.81	1576.81	0.05182	0.062786
31/12/2020	341.55414	183.68	1575.68	0.05181	0.062831

Table 3. Gaia EOL with 115 kg.

EOL epoch	Available Δv [m/s]	Fuel @EOL [kg]	Total mass [kg]	Area-to-mass [m2/kg]	Cr* Area-to-mass
06/07/2019	218.74	115	1507	0.054222179774300	0.065694658874829

5. Results for Gaia heliocentric disposal

This section presents the results of the heliocentric disposal for Gaia. Particular emphasis is given to highlight correlations between the optimised trajectory and the position of the Earth + Moon around the Sun when the manoeuvre is initiated. Indeed, as will be clear, this is an important parameter which influences the effectiveness of the disposal. We will indicate this parameter in terms of the true anomaly of the Earth + Moon around the Sun at time t_0, which is when the spacecraft leaves the LPO. Note that in the figures of the following subsections each point represents a fully optimised solution.

5.1. Results Gaia disposal design: Case 2.A

The first set of results consider a maximum available Δv_{EOL} of 343.52 m/s (corresponding to a propellant mass of 184.81 kg) on 06/07/2019 (i.e., after the eclipse avoidance manoeuvre) as in

Table 2. Moreover, for what concern the cost function to be minimised the case 2 was considered (see Section 3.2), which means that the cost function in Eq. (6) was checked on the points of the trajectory corresponding to close approaches as in Eq. (7) (see Table 4).

Table 4. Optimisation constraints of Run 1.

Cost function: J evaluated at close approaches	Δv_{EOL}	Simulation name
$J_{\mathrm{leg\,2,\,min}} = \min\left(J_{\mathrm{leg\,2}}\left(\mathbf{s}_{\mathrm{leg\,2,\,syn}} @ \mathrm{CA} \right) \right)$	343.52014 m/s	v 11
Case 2	Case A	

Figure 3 shows the value of the cost function in Eq. (6) as function of the true anomaly of the Earth + Moon around the Sun at time t_0, which is when the spacecraft leaves the LPO. A negative value of the cost function represents a more robust solution, as can be also seen from Figure 4, which represents the value of the minimum value of the Jacobi constant at close approaches as defined in Eq. (7) (dot symbol), the average value of the Jacobi constant over following close approaches (cross symbol) and the value of the Jacobi constant at the minimum distance from Earth (circle symbol). The solutions in Figure 3 and Figure 4 are colour-coded with respect to the minimum distance that each trajectory achieves from the Earth during the disposal time interval Δt_{EOL} . After the disposal manoeuvre Δv_2 is given, it is also possible to rank the disposal trajectories according to the minimum distance from Earth that the spacecraft attains along leg 2 (i.e., during Δt_{EOL}). This is recorded in Figure 5, where is interesting to note that a higher minimum distance from Earth is attained by those solutions which leave the LPO in correspondence of the Earth + Moon at a range of 180 to 360 degrees about the Sun. For all the solutions, the minimum distance from Earth is around $4 \cdot 10^6$ km and $J_{\mathrm{leg\,2,\,min}}$ is always above J_{L_2} . From Figure 3 to Figure 5 it is also interesting to note the comparison between the solution optimised over $\Delta t_{\mathrm{EOL}} = 30$ years (a) and the verification, through numerical integration, of the solution over 100 years (b). In this case, as expected, some of the correlation with the initial position of the Earth + Moon around the Sun is lost (as the solution is only optimised above 30 years not 100 years). Moreover, it is possible to see that the minimum distance from Earth is slightly decreased (i.e., between $3 \cdot 10^6$ km and $4 \cdot 10^6$ km), but always well above the L_2 to Earth distance, therefore, in all cases, a safe and robust disposal is achieved. If we look at the measure $J_{\mathrm{leg\,2,\,min}} - J_{L_2}$, we can note that, in some cases over 100 years (see Figure 3b and Figure 4b), the Hill's curve are open in correspondence of some close approaches. However, as shown in Figure 5b, the spacecraft is far away from L_2. Figure 6 represents the value of the Jacobi constant for each trajectory (i.e., initial time of the disposal). In particular, for each trajectory we show the minimum Jacobi constant over the subsequent close approaches (dot symbol), the average value of the Jacobi constant over following close approaches (cross symbol) and the value of the Jacobi constant at the minimum distance from Earth (circle symbol). The colouring code shows the initial position of the Earth + Moon around the Sun. Figure 7 aims at characterising the close

approaches. In particular, for each solution, the true anomaly of the Earth + Moon in correspondence of $J_{\text{leg 2, min}}$ and or the minimum distance of Gaia from the Earth are shown with a blue dot and a red cross respectively. Focusing on the simulation for 100 years, it is possible to note that $J_{\text{leg 2, min}}$ is attained when the Earth + Moon is in the first quadrant (i.e., $0 \leq f_{\text{Earth}} \leq 90$ degrees) or in the fourth quadrant (i.e., $270 \leq f_{\text{Earth}} \leq 360$ degrees), whereas the true anomaly of the Earth + Moon at the minimum distance Gaia-Earth shows a quasi-linear behaviour with the initial position of the Earth around the Sun.

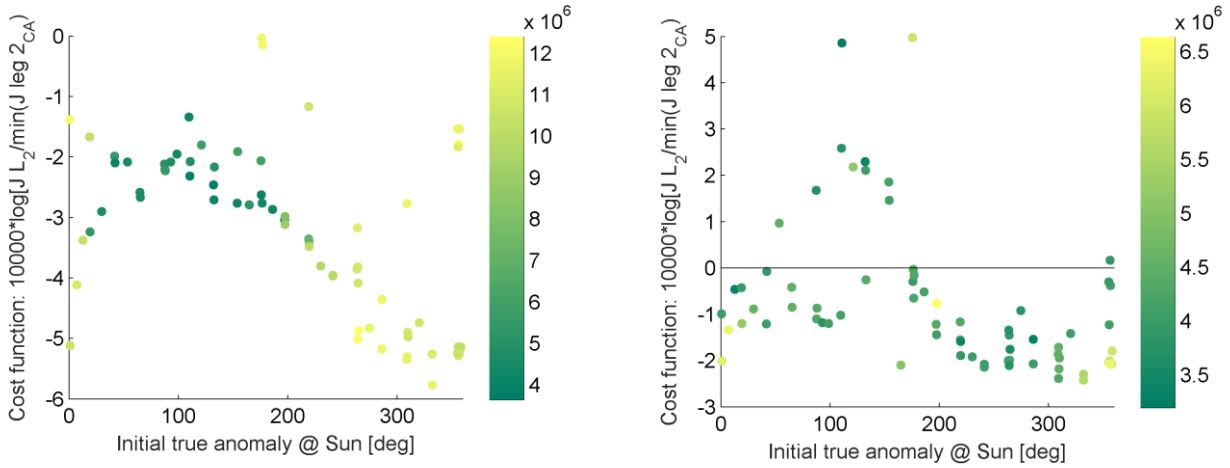

a) Optimisation with $\Delta t_{\text{EOL}} = 30$ years *b)* Verification with $\Delta t_{\text{EOL}} = 100$ years

Figure 3. Gaia heliocentric disposal: cost function depending on the angular position of the Earth + Moon when the disposal is initiated.

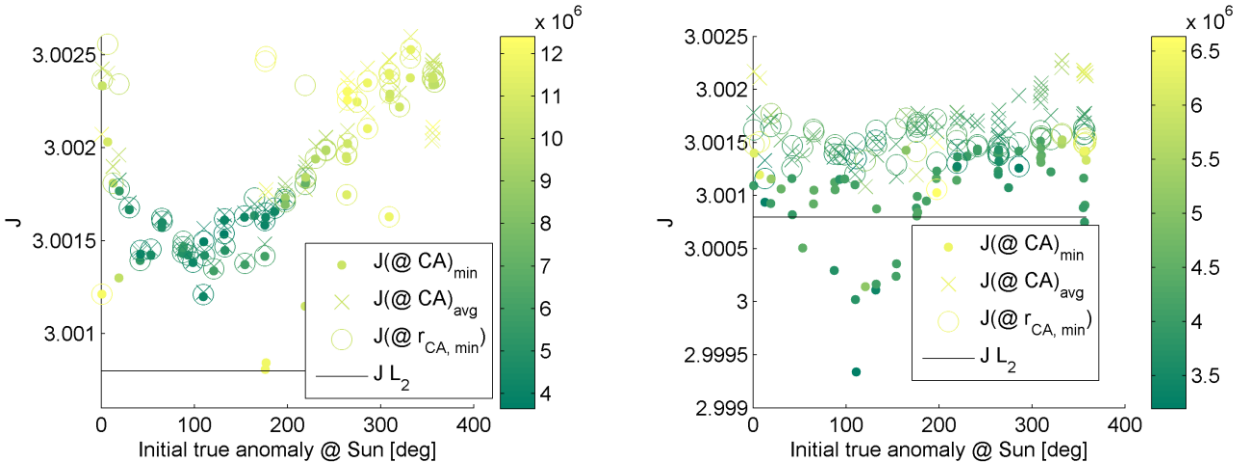

a) Optimisation with $\Delta t_{\text{EOL}} = 30$ years *b)* Verification with $\Delta t_{\text{EOL}} = 100$ years

Figure 4. Gaia heliocentric disposal: Jacobi constant as function of the angular position of the Earth + Moon when the disposal is initiated.

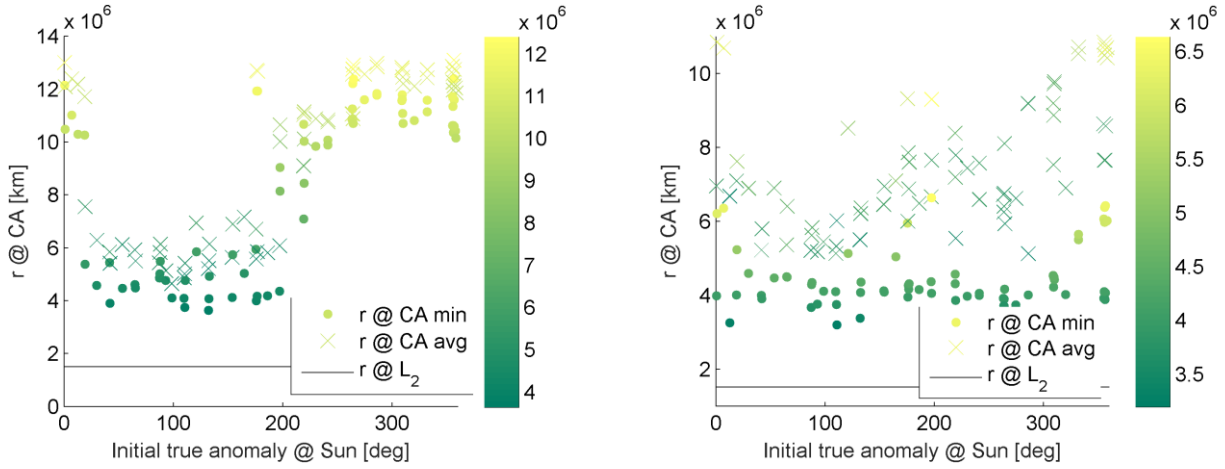

a) Optimisation with $\Delta t_{EOL} = 30$ years *b)* Verification with $\Delta t_{EOL} = 100$ years

Figure 5. Gaia heliocentric disposal: minimum distance from Earth as function of the angular position of the Earth + Moon when the disposal is initiated.

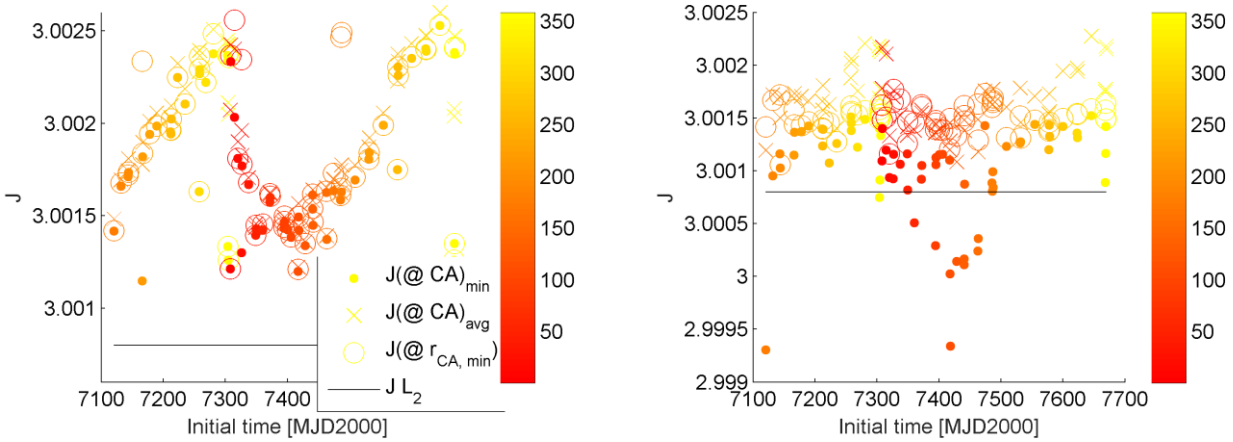

a) Optimisation with $\Delta t_{EOL} = 30$ years *b)* Verification with $\Delta t_{EOL} = 100$ years

Figure 6. Gaia heliocentric disposal: Jacobi constant as function of the time when the disposal is initiated.

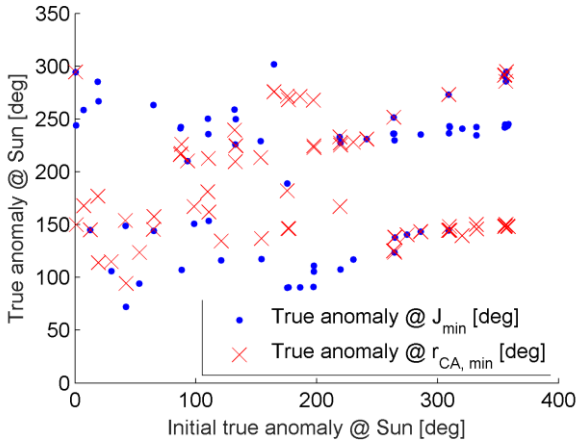

a) Optimisation with $\Delta t_{EOL} = 30$ years

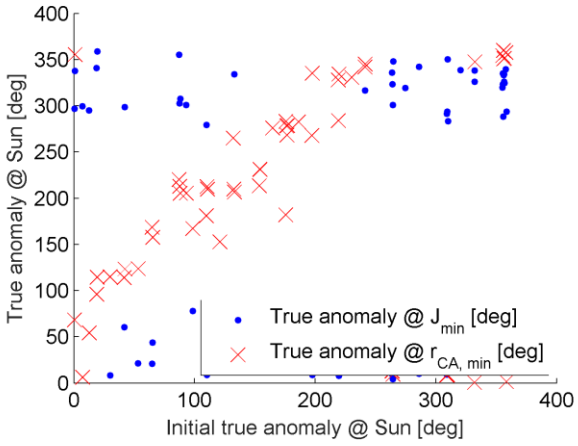

b) Verification with $\Delta t_{EOL} = 100$ years

Figure 7. Gaia heliocentric disposal: true anomaly of the Earth + Moon in correspondence of J_{min} and of r_{min}.

The next set of figures characterise the manoeuvre design selected via the optimisation. Figure 8 characterise the second Δv_2 manoeuvre. For all the solution Δt_1 is always around 5.8 months (Figure 8a) and the Δv_2 is given when the Earth + Moon is around the apogee (Figure 8b). Figure 9 represents for each solution the in-plane and out-of-plane angle of the first manoeuvre (in the synodic system). As it could be expected an in-plane angle between -90 and +90 degrees is chosen.

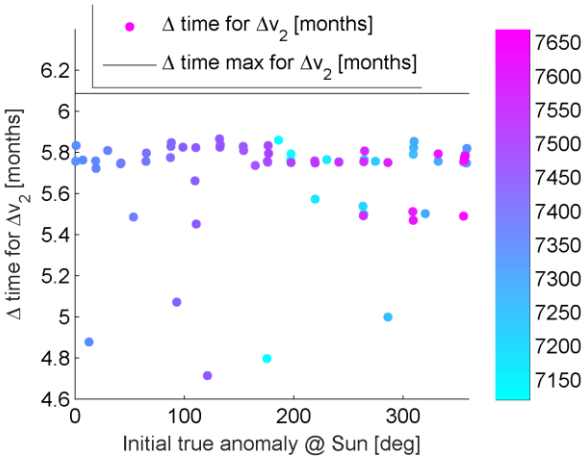

a)

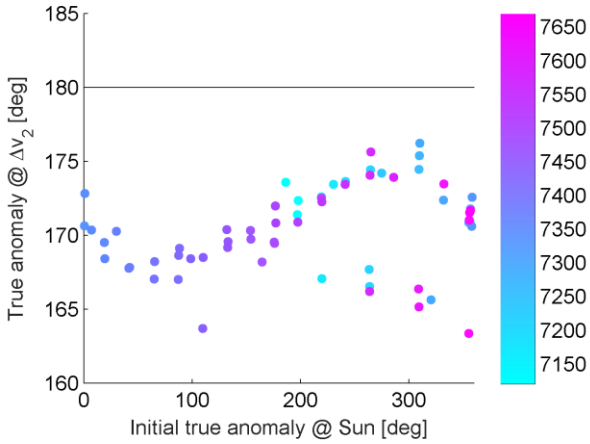

b)

Figure 8. Gaia heliocentric disposal: second manoeuvre. A) Δt_1 at which Δv_2 is given. B) True anomaly of the Earth in correspondence of when Δv_2 is given.

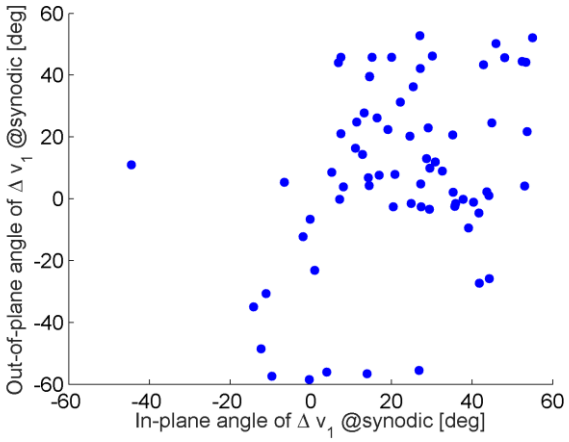

Figure 9. Gaia heliocentric disposal: in-plane and out-of-plane angle of the first manoeuvre (in the synodic system).

Finally Figure 10 shows how the maximum available Δv is divided between the first and the second manoeuvre, also considering the efficiency. For each solution is it is shown the theoretical value of Δv_1 (dot symbol) and the actual value after the efficiency evaluation (cross symbol). The theoretical value of Δv_2 is added to Δv_1 (circle symbol) to obtain the maximum available (black dot) as for all the simulation the whole available Δv is used. The actual value of Δv_2 , after efficiency evaluation is added on top to Δv_1 (with a x symbol). The reason why Δv_2 before and after efficiency is quite different may be due to the fact the direction of the second manoeuvre was fixed in the synodic system, but also due to the fact that in general a higher ratio is left to the second manoeuvre with respect to the first one. It is interesting to note how the allocation of available propellant between first and second manoeuvre depends on the time the spacecraft is injected on the disposal trajectory.

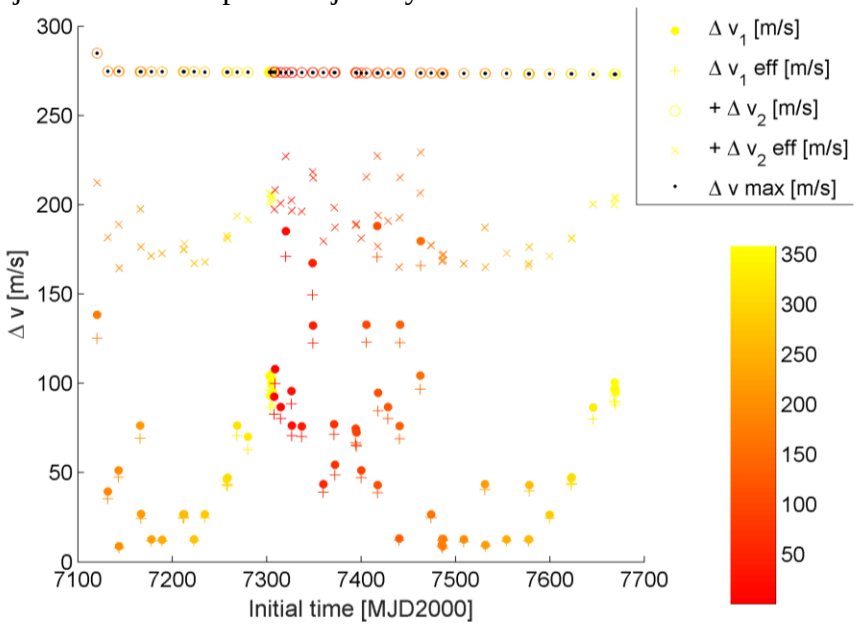

Figure 10. Gaia heliocentric disposal: Δv manoeuvre allocation.

5.1.1. Representative disposal solution departing on 7669 MJD2000

A representative solution[4] for disposal is here described. The same set of data and figures are available for all the solutions presented in the following sections. The selected solution departs from the LPO on 7669.19272665 MJD2000, corresponding to 2020/12/30 at 16:37:31.58, corresponding to a true anomaly of the Earth + Moon about the Sun of 356 degrees . The optimal design parameter for this solution is $\mathbf{y} = [0.3561 \quad 37.74 \text{ deg} \quad -0.16 \text{ deg} \quad 173.38 \text{ days}]$.

Figure 11 represents the evolution of the Jacobi constant along the disposal trajectory, in blue along the Leg 1 and in red along the Leg 2. It is possible to see the oscillations in the Jacobi constant due to the rotation of the Earth + Moon around the Sun (high-frequency oscillations scanned by crosses and x symbols represent the Earth's apogees and perigees). From the close-up in Figure 12 it is possible to see that the perigees falls close to the local minima of *J* (green cross symbols), the apogee in correspondence of the local maxima of *J* (red x symbols). Figure 11 shows also longer period oscillations that depend on the evolution of the trajectory in the Synodic system. In particular the maximum peaks are when the spacecraft is in the positive-*x* plane, the minimum peaks are when the spacecraft is in the negative-*x* plane. This means that the Hill's curves tend to be more open when the spacecraft is far away from the Earth (i.e., -x axis of the synodic plane) as *J* is below the value of the *J* at L_2. Along Leg 2, the condition at close approaches are also superimposed with a cyan cross and black dot. The condition of close approaches is also visible in Figure 13 that represents the distance between Gaia and the Earth and in Figure 14 that shows a close-up of the trajectory in the synodic system in vicinity of the L_2 point. As can be seen, the spacecraft is always outside the Hill's curves with respect to the L_2 point. The trajectory can be also represented in the Sun-centred inertial system (see Figure 15b) to appreciate that the disposal manoeuvres moves the spacecraft on an orbit which is far the Earth orbit. Leg 1 of the disposal is the equivalent to the transfer orbit from the Gaia orbit to the red orbit (i.e., Leg 2).

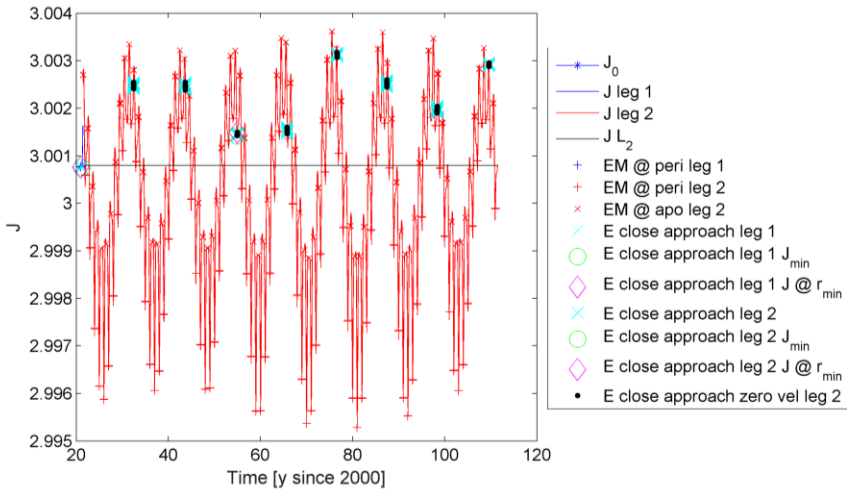

Figure 11. Gaia heliocentric disposal on 7669 MJD2000: Jacobi constant along the disposal trajectory.

[4] Run identifier: 1101.

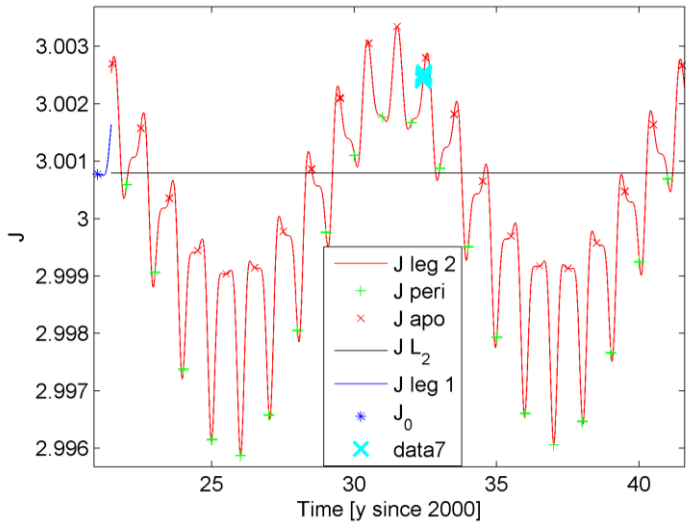

Figure 12. Gaia heliocentric disposal on 7669 MJD2000: close-up of the Jacobi constant along one part of the disposal trajectory.

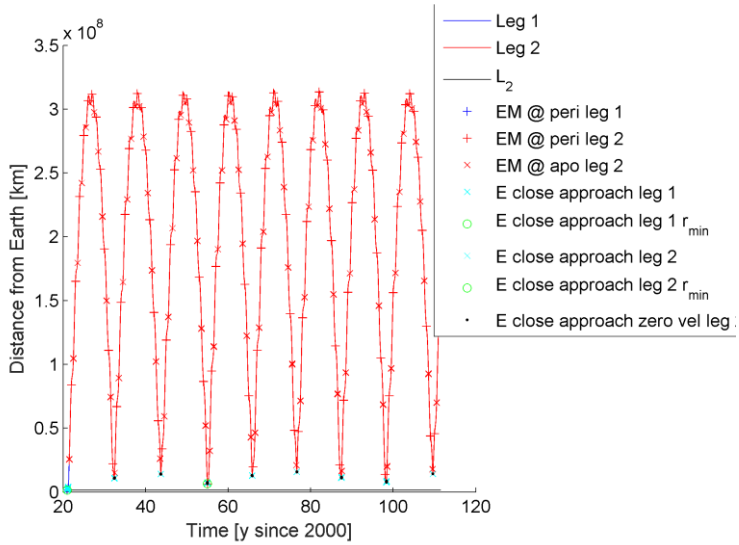

Figure 13. Gaia heliocentric disposal on 7669 MJD2000: distance from Earth along the disposal trajectory.

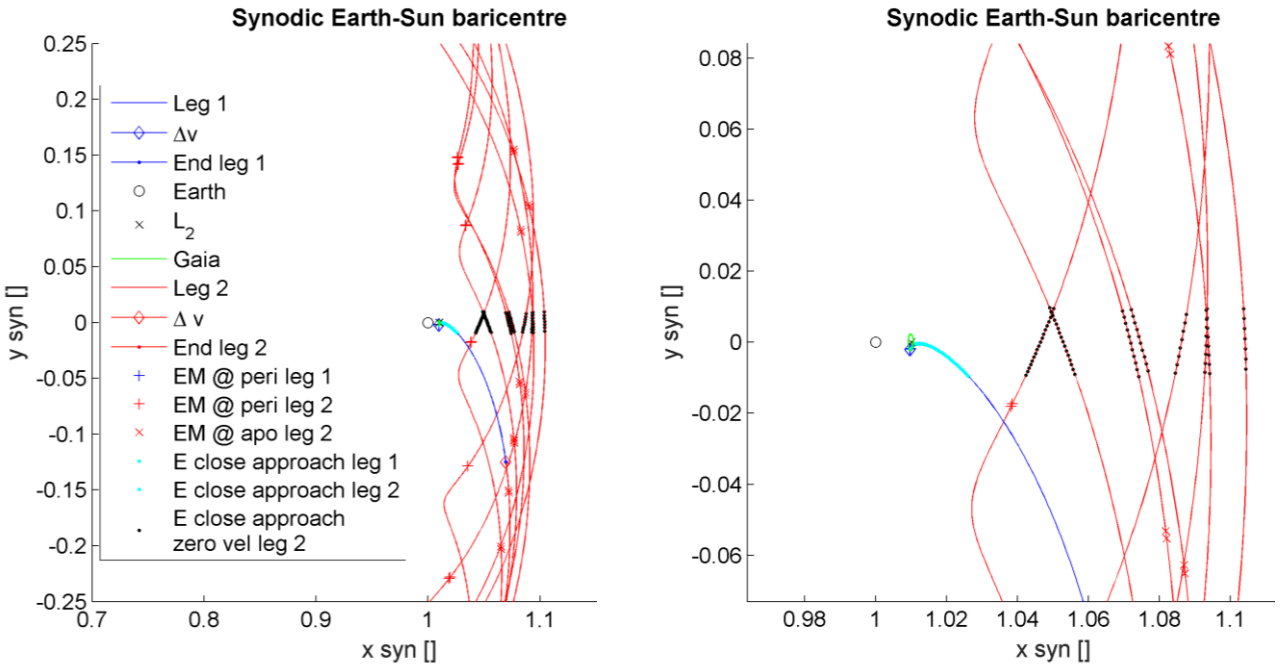

a) *b)*

Figure 14. Gaia heliocentric disposal on 7669 MJD2000: a) trajectory in the synodic system, b) close-up at L_2. The back circle is the Earth, the green line the LPO, the blue line leg 1 of the trajectory, the red line represents leg 2 of the trajectory.

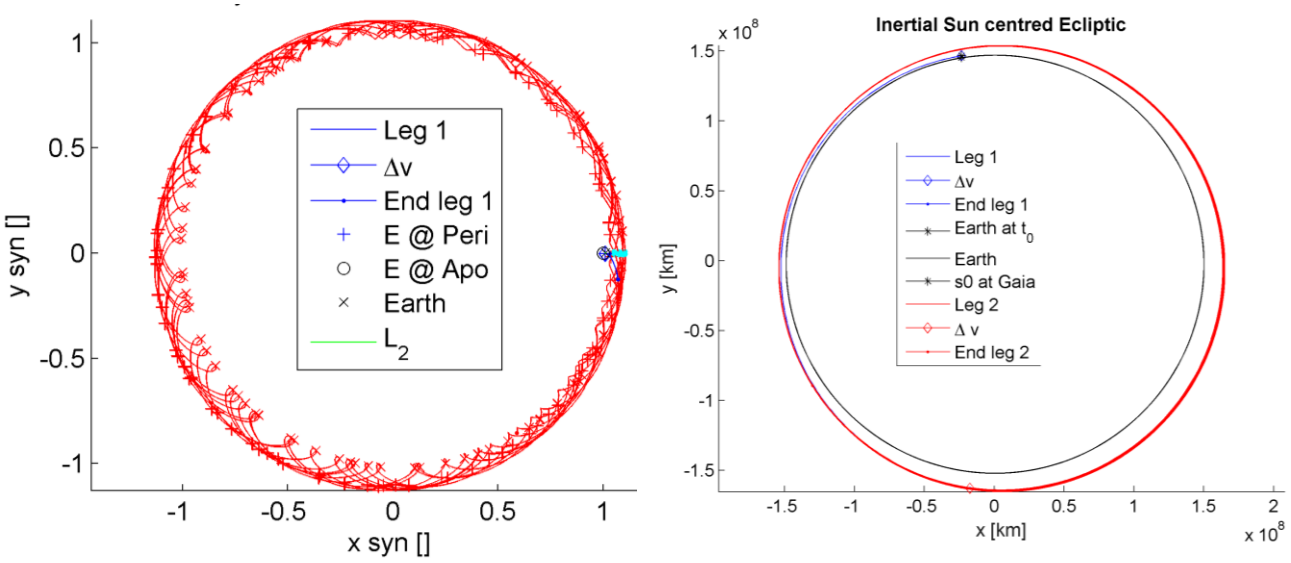

a) *b)*

Figure 15. Gaia heliocentric disposal on 7669 MJD2000: a) trajectory in the synodic system and b) trajectory in the Sun-centred ecliptic inertial system.

5.2. Results Gaia disposal design: Case 2.B

The second set of results consider a maximum available Δv_{EOL} of 218.74 m/s (corresponding to a propellant mass of 115 kg) on 06/07/2019 (i.e., after the eclipse avoidance manoeuvre) as in

Table 3. The cost function to be minimised is still computed on the points of the trajectory corresponding to close approaches as in Eq. (7) (see Table 5).

Table 5. Optimisation constraints of Run 2.

Cost function: J evaluated at close approaches	Δv_{EOL}	Simulation name
$J_{\text{leg 2, min}} = \min\left(J_{\text{leg 2}}\left(\mathbf{s}_{\text{leg 2, syn}}@\text{CA}\right)\right)$	218.74 m/s	v 11 B
Case 2	Case B	

The optimisation was performed for different starting time from the LPO, corresponding to different values of the true anomaly of the Earth + Moon around the Sun at time t_0. The value of the cost function in this case is lower in magnitude than case in Section 5.1 as now the maximum available Δv for disposal is lower. The disposal trajectories are then ranked according to the minimum distance from Earth in that the spacecraft attains along Leg 2 (i.e., during Δt_{EOL}) in Figure 16 (to be compared to Figure 5). In this case the minimum distance is very close to $3 \cdot 10^6$ km and $J_{\text{leg 2, min}}$ is always above J_{L_2} for the 30 years simulation. It is interesting to note the comparison between the solution optimised over $\Delta t_{EOL} = 30$ years (Figure 16a) and the verification, through numerical integration, of the solution over 100 years (Figure 16b). The minimum distance from Earth goes down to $2 \cdot 10^6$ km, but always well above the L_2 to Earth distance, therefore, in all cases, a safe disposal is achieved. If we look at the measure $J_{\text{leg 2, min}} - J_{L_2}$, we can note that, in some cases over 100 years, the Hill's curve are open in correspondence of some close approaches. However, as shown in Figure 16b, the spacecraft is still away from L_2.

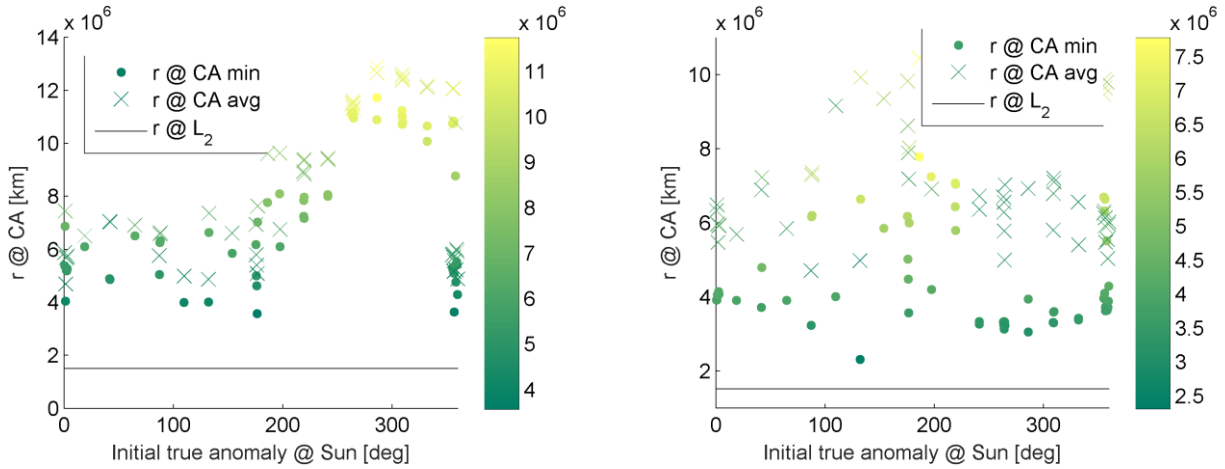

a) Optimisation with $\Delta t_{EOL} = 30$ years *b)* Verification with $\Delta t_{EOL} = 100$ years

Figure 16. Gaia heliocentric disposal: minimum distance from Earth as function of the angular position of the Earth + Moon when the disposal is initiated.

6. Effect of the Earth's eccentricity

In Section 3, the method for computing the manoeuvre required to close the zero-velocity curves in the CR3BP is summarised. As shown by [3, 6], the required increment in the Jacoby constant, ΔJ, depends on the distance of the spacecraft from the Earth. The required Δv is thus dependent on the selected trajectory, belonging to the unstable manifold, departing from the LPO and to the point along the trajectory in which the disposal manoeuvre is given.

When the effect of the Earth's orbit eccentricity is included, a margin in the Δv must be taken into account. Indeed, an additional energy term to the relative mechanical energy needs to be considered and the analytic representation of the zero velocity curves became problematic. In this case, as shown by Soldini et al. [9], depending on the approximation chosen for representing the zero-velocity curves, it can be difficult to predict whether, after the second manoeuvre, the zero velocity curves are effectively closed or not. This is due to the non-autonomous nature of the equations of motion in the Elliptical Restricted Three Body Problem (ER3BP), where an energy constant that describes the dynamics does not exist. Indeed, in the ER3BP, the energy along a trajectory depends on the initial true anomaly of the Earth when the spacecraft is injected on the unstable manifold, while it is conserved along a selected trajectory [9].

In ER3BP, the equations of motion are written in a non-dimensional, non-uniformly rotating and pulsating coordinates, where the motion of the Earth + Moon around the Sun is described by an ellipse under the two body approximation [7]. After the transformation of the orbit of Gaia from sidereal (i.e., full ephemeris model) to ER3BP synodic system, the modified Jacoby constant in the ER3BP is defined as:

$$J_{\mathrm{ER3BP}} = -\left(x'^2 + y'^2 + z'^2\right) + 2\Omega - 2\int_{f_0}^{f} \frac{e\sin f}{\left(1+e\cos f\right)^2} W df \tag{8}$$

where e is the eccentricity of the Earth's orbit around the Sun and f is the true anomaly Ω and W are defined respectively as:

$$\Omega = \frac{1}{1+e\cos f}\left[\frac{1}{2}\left(x^2+y^2-e\cos f z^2\right) + \left(1-\beta\right)\frac{1-\mu}{r_{\mathrm{S}}} + \frac{\mu}{r_{\mathrm{E}}}\right]$$

$$W = \left[\frac{1}{2}\left(x^2+y^2+z^2\right) + \left(1-\beta\right)\frac{1-\mu}{r_{\mathrm{S}}} + \frac{\mu}{r_{\mathrm{E}}}\right].$$

We can recognise in the right-hand side of Eq. (8) the first two terms, which are equal to the CR3BP case in Eq. (1) (with $e=0$ in the definition of the potential energy Ω and in the pulsating coordinates), while the integral term represents the additional term to be added to the relative mechanical energy with respect to the CR3BP case [9].

In the ER3BP, the manoeuvre for closure of the Hill's curves at L_2 is defined similarly to the CR3BP in Eq. (2) and the velocity after the manoeuvre in the ER3BP assumes the form:

$$\left(v_{ER3BP}{}^2\right)^+ = -J_{ER3BP\,L_2} - \Omega + 2\int_{f_0}^{f} \frac{e\sin f}{\left(1+e\cos f\right)^2} W df.$$

Note that, the location of the libration points is known and an analytical expression of the Jacoby constant for the libration points exists, $J_{ER3BP\,L_2}$, [9]. Thus, the condition of disposal is here express as for the CR3BP as $J_{ER3BP} > J_{ER3BP\,L_2}$. No approximations are here introduced because the additional energy along a selected trajectory can be computed numerically and it remains constant.

As mentioned before, the non-autonomous nature of the equations does not allow to find the exact representation of the zero velocity curves; thus, an approximated solution is needed. A comparison of different approximations of the zero velocity curves is given in [9], where it was demonstrated that the condition $J_{ER3BP} > J_{ER3BP\,L_2}$ holds and that after the closure the spacecraft reaches the energy of the pseudo libration point.

6.1. Analysis in the ERTBP

To perform an analysis on the long-term effect of the Earth's eccentricity, the constraints on the disposal manoeuvre in Section 4.2 are now relaxed. Four departures epoch for leaving Gaia orbit are selected, when the Earth + Moon barycentre is at $f_0 = 0$ deg (i.e., Earth + Moon at perigee), $f_0 = 90$ deg, $f_0 = 180$ deg (i.e., Earth + Moon at apogee) and $f_0 = 270$ deg. Note that the departing Δv on these manifold was not optimised in this case. For each solution, the dynamics is integrated for 15 years and the Δv required to close the curves along the trajectory in the ER3BP is computed at each time step using the ER3BP approximation and compared with the same solutions in the CR3BP. As for the C3RBP, a filter to identify the forbidden region is here included.

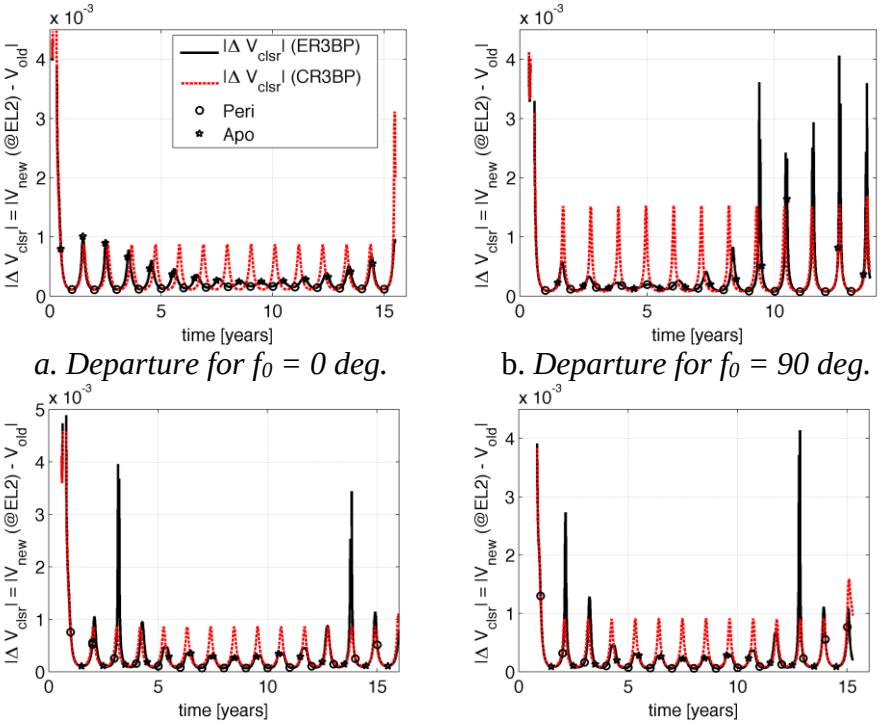

a. Departure for f_0 = 0 deg. b. *Departure for f_0 = 90 deg.*

c. *Departure for f_0 = 180 deg.* d. *Departure for f_0 = 270 deg.*

Figure 17. Δv required for disposal along the selected departure trajectory from Gaia's orbit. The dashed line is the Δv required in the CR3BP approximation, while the black continuous line is the approximation in the ER3BP. Along the disposal trajectory of the spacecraft, it is also shown the position of the Earth+Moon at the pericentre (circle) and apocentre (star).

Figure 17 shows a comparison of the required Δv in the CR3BP (dashed line) and the ER3BP (black continuous line) approximations respectively. The solution is similar for manoeuvre times

close to the LPO departure, where the discontinuity in the solution is due to the discarded solutions that after the deployment are in the forbidden region. In both cases, the solutions are oscillating along the disposal trajectory due to the effect of the spacecraft distance from the centre of mass that for the Sun – Earth + Moon system is circa in the Sun. When the spacecraft is far away from the close approach, that in this case appended after 15 years, the peaks in the required Δv have a repeating behaviour for the CR3BP, while a drift in the peaks and different amplitude of the peaks can be spotted for the ER3BP approximation. This can be explained since the solution in the required Δv in the ER3BP depends on the distance of the spacecraft from the centre of mass, on the Earth true anomaly and the position angle with respect to the barycentre of the synodic system. It is important to note that with a more accurate model, the required Δv can be very different from the CR3BP thus an uncertainty analysis of the probability of re-entry at the close approach is required when considering a high fidelity model.

7. Conclusions

The paper proposes a strategy for the design of the heliocentric disposal of Libration Point Orbits in the full-dynamical model. An energy method is applied to decrease the energy below the energy of the Libration point L_2, to close the way through the gateway for an Earth re-entry. The verification of the change in the Jacobi constant for the energy design approach is applied only in correspondence of close approaches to optimise the available Δv on board for achieving a sustainable and robust disposal in the following 100 years. A possible improvement of the optimisation consists in removing the constraints on the value of the angles for the second manoeuvre α_2 and β_2: as this should reduce the efficiency loss observed in Figure 10. Moreover, in a future work, the optimisation will be run on the full time window of 100 years: in this case, the results for the Case B formulation (check only on the close approaches) should tend towards the results of the Case A (check on all points) as more close approaches are registered. To this aim a fast numerical propagator for the trajectory in the full dynamics model is currently under development.

8. References

[1] Colombo, C., Alessi, E. M., Weg, W. v. d., Soldini, S., Letizia, F., Vetrisano, M., Vasile, M., Rossi, A. and Landgraf, M., "End-of-Life Disposal Concepts for Libration Point Orbit and Highly Elliptical Orbit Missions," *Acta Astronautica*, 2014, in press. doi: 10.1016/j.actaastro.2014.11.002

[2] Colombo, C., Letizia, F., Soldini, S., Lewis, H., Alessi, E. M., Rossi, A., Vasile, M., Vetrisano, M. and Van der Weg, W., "End-of-Life Disposal Concepts for Lagrange-Point and Highly Elliptical Orbit Missions," 2014.

[3] Colombo, C., Letizia, F., Soldini, S., Alessi, E. M., Rossi, A., Dimare, L., Vasile, M., Vetrisano, M. and Van der Weg, W., "End-of-Life of Gaia Mission and Lisa Pathfinder Mission: Heliocentric Disposal and Earth Re-Entry Options," 2014.

[4] Alessi, E. M., "The Reentry to Earth as a Valuable Option at the End-of-Life of Libration Point Orbit Missions," *Advances in Space Research*, Vol. 55, No. 12, 2015, pp. 2914-2930. doi: 10.1016/j.asr.2015.03.012

[5] Canalias, E., "Contributions to Libration Orbit Mission Design Using Hyperbolic Invariant Manifolds," Ph.D. Thesis, Universitat Politècnica de Catalunya, 2007.

[6] Olikara, Z. P., Gómez, G. and Masdemont, J. J., "Dynamic Mechanisms for Spacecraft Disposal from Sun–Earth Libration Points," *Journal of Guidance Control and Dynamics*, Vol. 0 No. 0, in press 2015, pp. 1-14. doi: 10.2514/1.G000581

[7] Sezebehely, V., *Theory of Orbits in the Restricted Problem of the Three Bodies*, New York, 1967.

[8] Cobos, J. and Masdemont, J. J., "Astrodynamical Applications of Invariant Manifolds Associated with Collinear Lissajous Libration Orbits," *Proceedings of the Conference Libration Point Orbits and Application*, 2003, pp. pp. 253-268.

[9] Soldini, S., Colombo, C. and Walker, S., "Solar Radiation Pressure End-of-Life Disposal of Satellite in the Elliptic Restricted Three Body Problem: Application to Gaia Mission," *Celestial Mechanics and Dynamical Astronomy*, under review 2015.